Electronic Supplementary Material (ESI) for Nanoscale Horizons.

- Supporting Information –

Evolution of Adsorption Heights in the On-Surface Synthesis and Decoupling of Covalent Organic Networks on Ag(111) by Normal-Incidence X-ray Standing Wave

Lukas Grossmann[1,2], David A. Duncan[3], Samuel P. Jarvis[4], Robert G. Jones[5], Soumen De[6], Johanna Rosen[7], Michael Schmittel[6], Wolfgang M. Heckl[1,2], Jonas Björk[7], and Markus Lackinger[1,2*]

[1]Deutsches Museum, Museumsinsel 1, 80538 München, Germany

[2]Technische Universität München, Physics Department, James-Franck-Strasse 1, 85748 Garching, Germany

[3]Diamond Light Source, Harwell Science and Innovation Campus, Didcot OX11 0QX, U.K.

[4]Lancaster University, Physics Department, Lancaster LA1 4YB, U.K.

[5]University of Nottingham, Department of Physical Chemistry, School of Chemistry, Nottingham NG7 2RD, U.K.

[6]Center of Micro and Nanochemistry and Engineering, Organische Chemie I, Universität Siegen, Adolf-Reichwein-Str. 2, 57068 Siegen, Germany

[7]Linköping University, Department of Physics, Chemistry and Biology, IFM, 581 83 Linköping, Sweden.

Table of Contents

1. Materials and methods

1.1. Sample preparation and general remarks

Two different Ag(111) single crystals were used as substrates for STM and XPS / NIXSW experiments. They were prepared by cycles of Ar^+ ion sputtering and annealing at ~500 °C. The surface cleanliness was verified prior to each experiment by either STM or XPS. The synthesis and characterization of the 2,4,6-tris(4-bromophenyl)-1,3,5-triazine (TBPT) precursor is described in section 6. TBPT was deposited from a home-built evaporator at 195 °C crucible temperature for 7 min and 15 min for low and high coverage XPS / NIXSW experiments, respectively. The coverages were calibrated by STM experiments. Comparable coverages were achieved for XPS / NIXSW experiments by carrying out the deposition with the same evaporator using similar parameters at identical distance between evaporator and sample. Two independent experimental runs were conducted with ~15% (low coverage, main manuscript) and ~30% (high coverage, Supporting Information) coverages with respect to a regular organometallic phase (i.e. a hexagonal structure with a = b = 2.60 nm and two molecular entities per unit cell, corresponding to 0.52 carbon and 0.074 nitrogen atoms per Ag atom of the topmost Ag(111) layer, respectively). We intentionally used low coverages to avoid influences from molecular crowding that may play a role at higher coverages. After deposition of molecules, a homogenous coverage across the sample was verified by several XPS measurements that were conducted after macroscopically moving the sample.

At the synchrotron, annealing temperatures were estimated with the aid of a heater calibration curve. In the low coverage run, the organometallic phase was prepared by aiming at 200 °C for 23 min and monitoring the Br 2p core level by XPS. The heating was stopped when the molecularly bound bromine species at higher binding energy had completely vanished. By contrast, in the high coverage run the heater was aiming at 300 °C and the C 1s core level of the bromine carrying carbon atoms was monitored by XPS. The higher annealing temperature and the less pronounced signature of debromination in C 1s as a high binding energy shoulder unfortunately resulted in an already partial covalent network. For the conversion from organometallic to covalent we aimed at 500 °C for 20 min and monitored C 1s. The annealing step was terminated just as the organometallic shoulder originating from C_{Ag} reached its minimum. Iodine intercalation was carried out in a separate preparation chamber using a sample temperature of 350 °C and an iodine pressure of 10^{-6} mbar. After heating for 20 min, samples were allowed to cool down in the iodine atmosphere for additional 10 min.

1.2. STM

STM images were acquired at room temperature using a home-built low-temperature STM operated by a BP4 control system (Nanonis). Electrochemically etched tungsten tips were used and occasionally conditioned by Ar^+ ion sputtering. Stated tunneling voltages refer to the sample. STM images were processed by levelling and Gaussian filtering using Gwyddion v2.56.[1] For temperatures below 200 °C sample heating was carried out radiatively with temperatures estimated from a heater

calibration curve. For temperatures above 200 °C e-beam heating was used and sample temperatures were measured with an infrared pyrometer. Iodination was carried out in a separate preparation chamber with an iodine pressure of 5×10^{-7} mbar for 5 min. Elevated sample temperatures were used for iodination by preheating the sample to ~350 °C in the main chamber and swiftly transferring the sample to the likewise preheated sample stage in the iodination chamber. Successful iodine intercalation could be directly verified by STM imaging (main manuscript). The STM measured triazine-to-triazine distances stated in the main manuscript represent average values of 6, 11 and 13 independent measurements carried out in virtually drift-free images for the organometallic, covalent and decoupled networks, respectively. Eventually, we assumed a 2% calibration error (as judged from checking the calibration with the lattice of the Ag(111) surface) since the statistical error was smaller.

1.3. XPS / NIXSW

XPS and NIXSW experiments were carried out at the Diamond Light Source at the Beam Line I09[2] in the Experimental Hutch 2. This beamline consists of two independent branches for soft (0.1 - 1.8 keV) and hard x-rays (2.1 - 15 keV). Each branch has its own monochromator, specifically a plane grating monochromator and a double Si single crystal monochromator (DCM), respectively. Photoelectrons were detected by a Scienta EW4000 HAXPES hemispherical electron analyzer with the sample held at room temperature. The analyzer was mounted perpendicular to the incident light in the same plane as the photon polarization (linear horizontal). The X-ray reflectivity was measured via a CCD camera as the light intensity emitted from a fluorescent plate that was mounted on the same port through which the incident X-rays passed. Prolonged measurements on the same spot indicated minor beam damage. To still minimize potential beam damage, NIXSW measurements were carried out on multiple independent spots and averaged (typically 4...10 spectra for the dilute C and N species, and 1…3 for Br and I. XP spectra were recorded using soft X-rays with photon energies of: 770 eV for I 3d; 550 eV for N 1s; 435 eV for C 1s; 330 eV for Br 2p. Binding energies refer to the Fermi edge, which was measured at the same photon energy and obtained from fitting with a sigmoid function. XP spectra were fitted with a Shirley background and Voigt profiles using the software fityk v.1.3.3.[3] NIXSW photoelectron yield curves were acquired for C 1s, N 1s, Br 3p and I 3d core levels for the 111 reflection of the Ag(111) substrate over a photon energy range of ~11 eV around the Bragg energy of ~2.62 keV. Before each NIXSW experiment a reflectivity curve of the 111 Bragg-reflection was acquired to verify high crystal quality at the measured sample region and to recenter the photon energy scan region to ensure that all scans were performed over the same photon energy scale with respect to the Bragg energy. Reflectivity curves were also acquired synchronously to the NIXSW spectra. These were fitted in order to define the energy scale relative to the Bragg energy, as well as to assess the experimental broadening induced by imperfections in both the DCM and the Ag(111) substrate.

For fitting the XPS peaks from the NIXSW experiments a Doniach-Sunjic (D-S) line profile was convoluted with a Gaussian, the former modeling broadening due to core hole lifetime, the latter

modeling experimental broadening. Each peak in a spectrum was assumed to have the same D-S width (and D-S asymmetry) but may have differing Gaussian widths. Each peak also has an associated step function (Gaussian error function), whose width is the same as the Gaussian width of the associated peak and whose height is a product of the associated peaks' intensity and a rescaling factor that is kept constant for all peaks. The background was modeled by a straight line, whose gradient and offset were both fitting parameters. Across the full photon energy range of a NIXSW measurement, only the intensity of the peaks and the gradient and offset of the background were allowed to vary.

The measured profile is then fitted uniquely, using dynamical diffraction theory,[4] by two dimensionless parameters: the coherent fraction, f_H, and the coherent position, P_H.[5] Non-dipolar effects in the angular dependence of the photoemission were taken into account by a backward-forward asymmetry parameter, Q, which was calculated theoretically using the average angle acquired on the analyzer (Θ = 18°, as defined in ref 6).

It is noteworthy that the analysis of the N 1s photoelectron yield curves was complicated due to a broad loss feature of the Ag(111) surface that also varied with the phase of the standing wave and changed upon iodination. To account for this feature we subtracted a smoothed averaged background curve acquired from a clean Ag(111) sample. This resulted in XP spectra with a remaining linear background that was fitted by the standard procedure.

1.4. Computational details

Periodic DFT calculations were carried out with the VASP code[7] using the projector-augmented wave method to describe ion-core interactions[8] and with planewaves expanded to a kinetic energy cutoff of 400 eV. The van-der-Waals density functional[9] described exchange-correlation effects, with the version by Hamada denoted as rev-vdWDF2.[10] The Ag(111) surface was described by a four layered slab using the computationally optimized fcc lattice parameter of 4.093 Å. The reaction byproduct, i.e. chemisorbed bromine atoms, were not considered in our calculations, neither as co-adsorbate on pristine Ag(111) nor in the iodine decoupling layer.

For the calculation of the organometallic dimer a $p(12 \times 11)$ surface unit cell was used. To employ periodic boundary conditions, we assumed commensurability of the covalent networks with both the Ag(111) surface and the iodine superstructure. To minimize the strain in the covalent network, we matched a $p(2 \times 2)$ supercell of the covalent network on a $(\sqrt{228} \times \sqrt{228})R \pm 6.6°$ supercell of the Ag(111) surface described by:

$$\begin{pmatrix} 14 & 2 \\ -2 & 16 \end{pmatrix} \begin{pmatrix} \vec{a}_1 \\ \vec{a}_2 \end{pmatrix}$$

where $\vec{a}_1$ and $\vec{a}_2$ are the surface unit cell vectors of Ag(111), using the convention $\vec{a}_1 = (a,0)$ and $\vec{a}_2 = \left(\frac{1}{2}a, \frac{\sqrt{3}}{2}a\right)$. This resulted in less than 1% compressive strain of the adsorbed covalent network as compared to the optimized free-standing covalent network. Furthermore, this surface unit cell is also

commensurate with the $\sqrt{3} \times \sqrt{3} \pm 30°$ iodine superstructure. For the calculations of the organometallic dimer and the covalent network on the Ag(111) surface (with or without iodine), only the Γ-point was used to sample the 1st Brillouin zone. For the calculations of iodine and bromine monolayers $\sqrt{3} \times \sqrt{3} \pm 30°$ superstructures were used with a 12×12 *k*-point sampling. All structures were geometrically optimized until the residual forces on all atoms (except the two bottom layers of the Ag(111) slab which were kept fixed) were smaller than 0.01 eV/Å.
Adsorption heights were calculated with respect to the bottom layer of Ag(111) according to:

$$h_{DFT}^{ad} = z_{ad} - z(m^{th}\ layer) - (m-1)d_{111}(Ag), \quad (1)$$

where z_{ad} is the z-coordinate of the adsorbate atom of interest, $z(m^{th}\ layer)$ is the z-coordinate of the m^{th}surface layer, and $d_{111}(Ag)$ is the Ag(111) bulk lattice plane spacing. The m^{th} layer is defined as the first fixed layer in the slab, in our case, $m = 3$. This definition is used as it better complies to NIXSW experiments, which measure adsorption heights with respect to the extended bulk lattice planes. Test calculations on bromine and iodine monolayers (Fig. S8 and Fig. S9) show that the adsorption heights are converged with respect to the number of layers of the Ag slab within 0.01 Å for four layers.

Adsorption energies E_{ads} were computed as:

$$E_{ads} = (E_{network@surf} - E_{network} - E_{surf}) / N_{mon},$$

where $E_{network@surf}$ is the total energy of the network on the surface (iodinated or bare Ag(111)), $E_{network}$ is the total energy of the free-standing covalent network, E_{surf} is the total energy of the surface (iodinated or bare Ag(111)), and N_{mon} is the number of monomeric units per unit cell in the network to which the stated adsorption energies were normalized.

STM simulations were conducted within the framework of the Tersoff-Hamann approximation.[11] Therefore, the tunneling current was expressed as the local density of states integrated between the Fermi level and the energy corresponding to the bias voltage in the experiments.[12] Accordingly, negative (positive) energy values correspond to filled (empty) state images acquired at negative (positive) sample bias.

2. Additional STM results

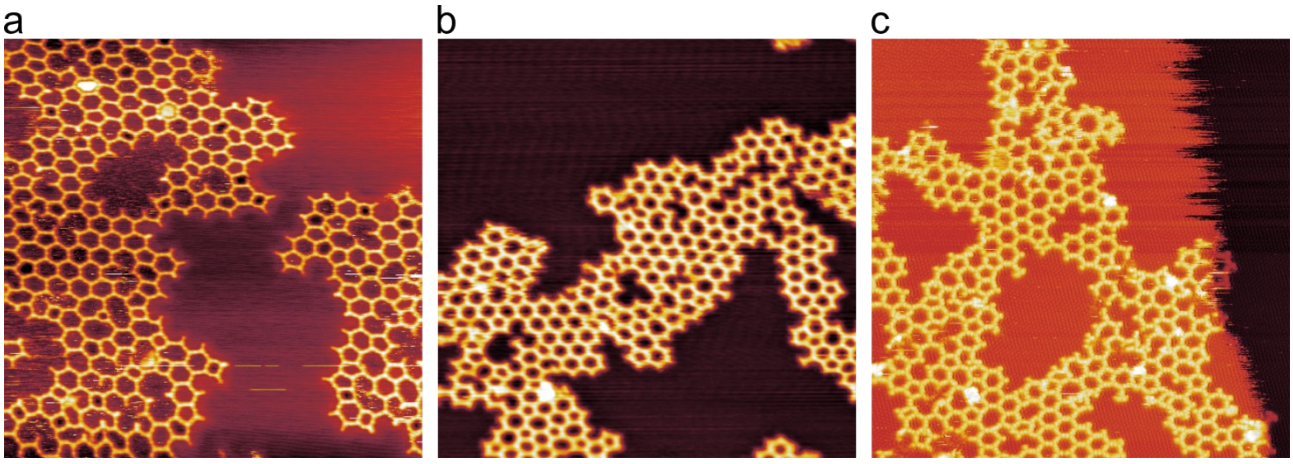

Fig. S1 Overview STM images acquired for **a)** organometallic networks, **b)** covalent networks directly on Ag(111), and **c)** covalent networks after intercalation of an iodine monolayer (Size of all STM image: 50 × 50 nm²; tunneling parameters: a +1.0 V, 30 pA; b +1.0 V, 30 pA; c -0.80 V, 80 pA).

3. Additional data of low coverage run

3.1. Additional XPS results

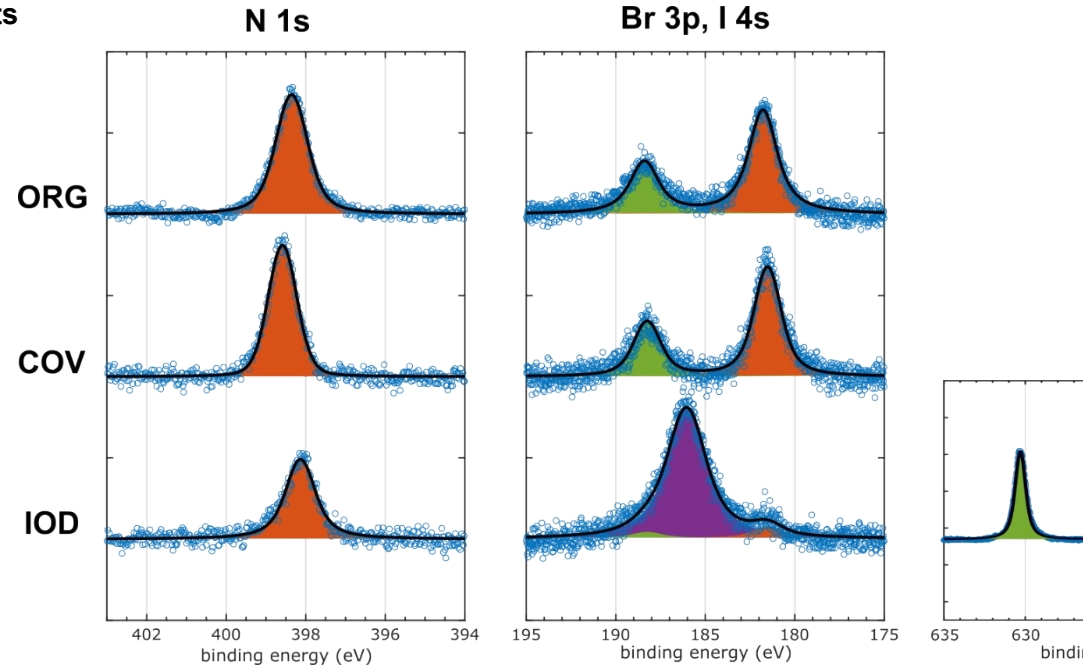

Fig. S2 XP spectra of N 1s, Br 3p, I 3d acquired in the low coverage run discussed in the main manuscript. ORG and COV denote the initial organometallic and subsequent covalent phase, respectively. IOD refers to the iodine intercalated sample state. N 1s consistently shows a single species. Br 3p shows only one doublet corresponding to a surface bound species for fully debrominated ORG and remains similar for COV. Upon iodination a strong I 3d doublet emerged, corresponding to chemisorbed iodine. Since the iodination was carried out at relatively high temperatures at the synchrotron, Br was mostly desorbed for IOD. Moreover, the Br 3p BE region overlaps with I 4s (186 eV BE) that emerged after iodination.

3.2. NIXSW results for N, Br, I

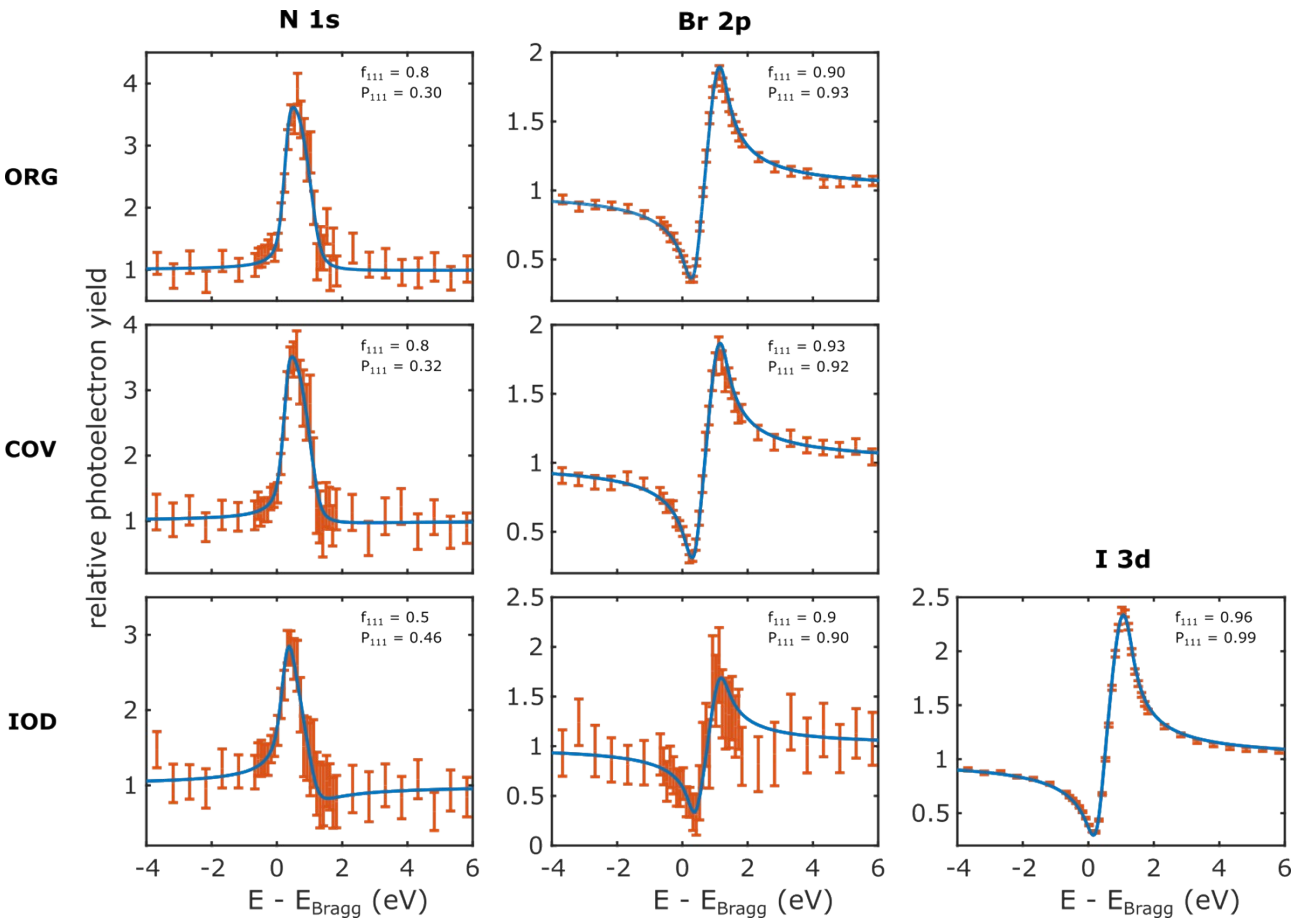

Fig. S3 Additional NIXSW data from the low coverage run discussed in the main manuscript. Photoemission yield curves of N 1s, Br 2p, I 3d for organometallic (ORG) and covalent networks directly on Ag(111) (COV) as well as after iodine intercalation (IOD). Data points are plotted in red and the error bars correspond to the standard error in the fit of the individual XP spectra at two standard deviations. The blue lines represent fits with the corresponding f_{111} and P_{111} indicated.

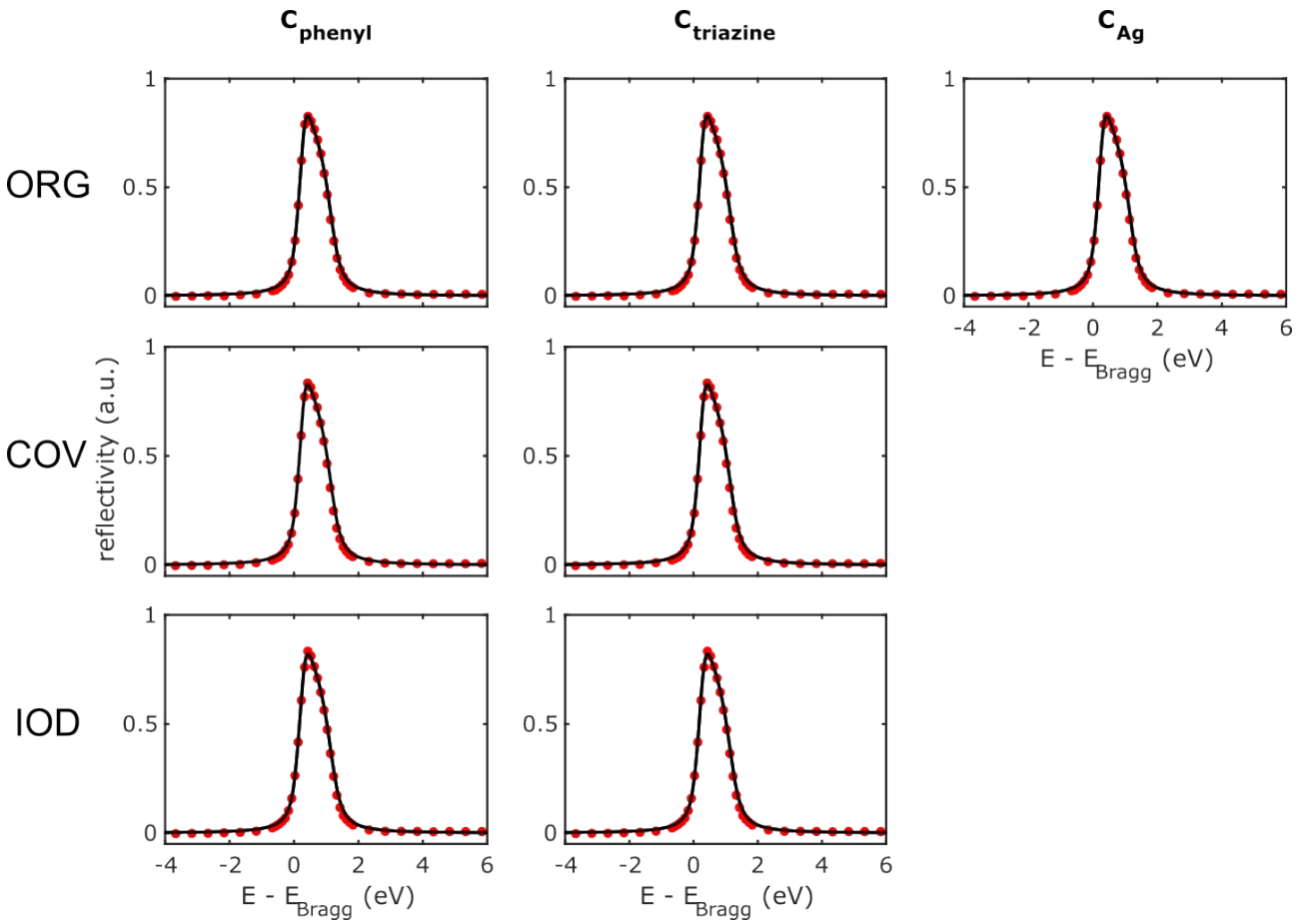

Fig. S4 Reflectivity curves exemplarily shown for the low coverage C 1s run. The X-ray reflectivity was simultaneously acquired with the NIXSW spectra from a fluorescent plate via a CCD camera. Red dots represent data points. The black lines are fits that were used to define the energy scale relative to the Bragg energy and to account for experimental broadening.

4. Additional data for high coverage run

4.1. XPS results

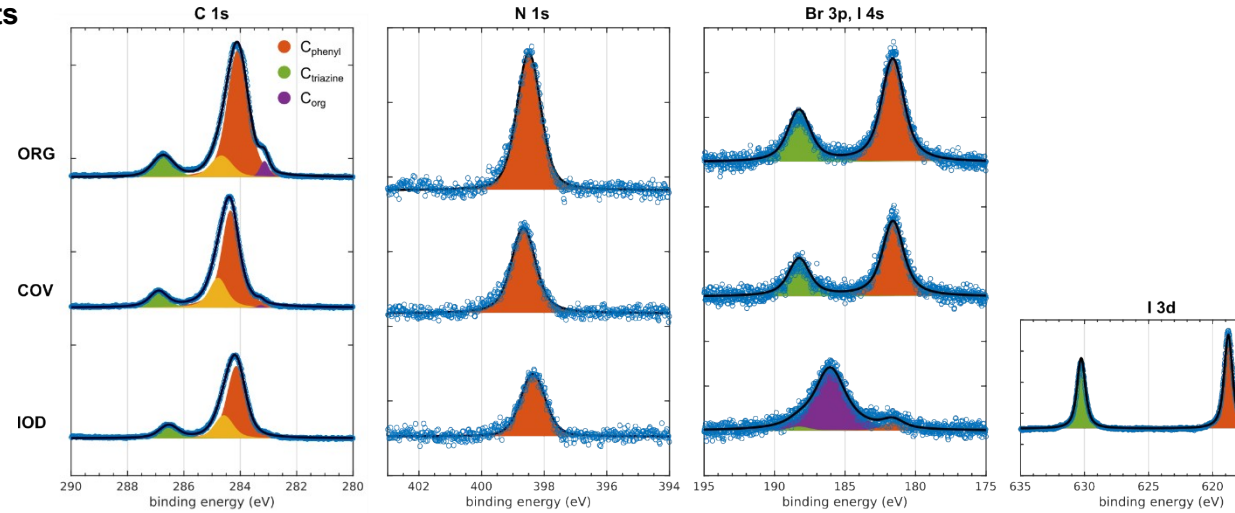

Fig. S5 C 1s, N 1s, Br 3p (I 4s) and I 3d XP spectra from the high coverage (~30%) run for organometallic (ORG) and covalent networks directly on Ag(111) (COV) as well as after iodine intercalation (IOD). These results reflect those of the low coverage run.

4.2. NIXSW results

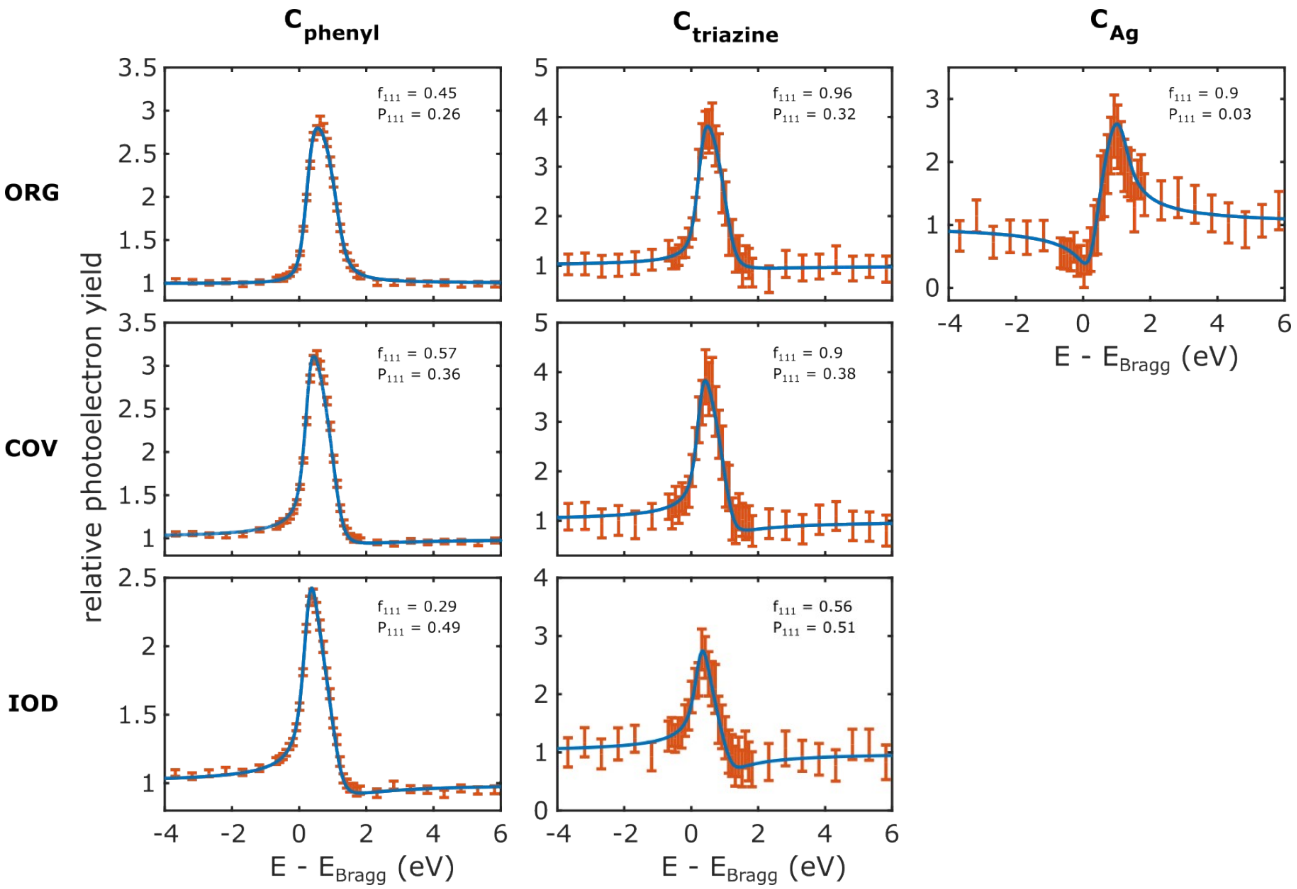

Fig. S6 C 1s NIXSW data from the high coverage run. Photoemission yield curves of the chemically distinct carbon species for organometallic (ORG) and covalent networks directly on Ag(111) (COV) as well as after iodine intercalation (IOD). Data points are plotted in red and the error bars correspond to the standard error in the fit of the individual XP spectra at two standard deviations. The blue lines represent fits with the corresponding f_{111} and P_{111} indicated. See Table S1 for a summary of results and their direct comparison to the low coverage run.

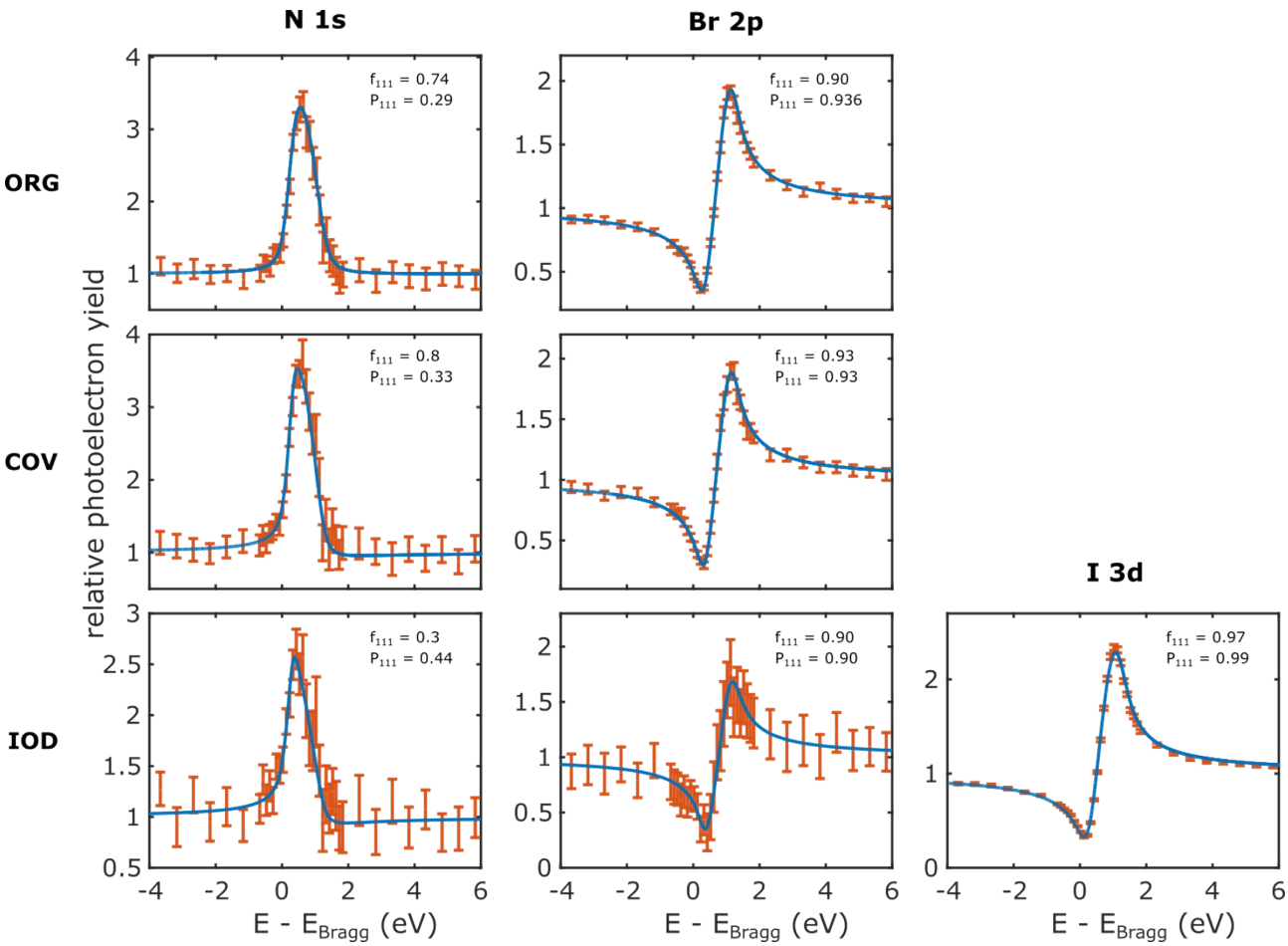

Fig. S7 Additional NIXSW data from the high coverage run. Photoemission yield curves for N 1s, Br 2p, I 3d for organometallic (ORG) and covalent networks directly on Ag(111) (COV) as well as after iodine intercalation (IOD). Data points are plotted in red and the error bars correspond to the standard error in the fit of the individual XP spectra at two standard deviations. The blue lines represent fits with the corresponding f_{111} and P_{111} indicated. See Table S1 for a summary of results and direct comparison to the low coverage run.

Table S1 Summarized NIXSW adsorption heights from the high coverage run. Coherent fractions f_{111} and coherent positions P_{111} for all species and sample stages. Adsorption heights were calculated as $h^{ad}_{exp} = (n + P_{111}) * d_{Ag(111)}$, with $d_{Ag(111)} = 2.354$ Å. The integer n was chosen to yield meaningful results: n=0 for Br and I; n=1 for C_{Ag}, C_{phenyl}, $C_{triazine}$ and $N_{triazine}$ before iodination: n=2 for C_{phenyl}, $C_{triazine}$ and $N_{triazine}$ after iodination to account for the intercalated iodine layer. For comparison the results from the low coverage run are shown on the right-hand side. It is noteworthy that the organometallic phase in the high coverage run was already partially covalent, which may explain the discrepancies.

			high coverage			low coverage		
sample stage	**core level**	**species**	**f_{111}**	**P_{111}**	h^{ad}_{exp}(Å)	**f_{111}**	**P_{111}**	h^{ad}_{exp}(Å)
organometallic	C 1s	phenyl	0.45 ± 0.03	0.26 ± 0.02	2.96 ± 0.04	0.56 ± 0.03	0.19 ± 0.02	2.81 ± 0.04
		organometallic	0.9 ± 0.2	0.03 ± 0.05	2.4 ± 0.2	1.0 ± 0.2	0.96 ± 0.07	2.3 ± 0.2
		triazine	0.96 ± 0.08	0.32 ± 0.04	3.1 ± 0.1	0.9 ± 0.2	0.34 ± 0.06	3.1 ± 0.2
	N 1s	triazine	0.74 ± 0.8	0.29 ± 0.04	3.0 ± 0.1	0.8 ± 0.2	0.30 ± 0.07	3.1 ± 0.2
	Br 2p	surface-bound	0.90 ± 0.02	0.936 ± 0.008	2.20 ± 0.02	0.90 ± 0.03	0.93 ± 0.01	2.19 ± 0.03
covalent	C 1s	phenyl	0.57 ± 0.05	0.36 ± 0.03	3.19 ± 0.06	0.56 ± 0.04	0.31 ± 0.02	3.08 ± 0.05
		triazine	0.9 ± 0.1	0.38 ± 0.04	3.2 ± 0.1	0.8 ± 0.2	0.35 ± 0.09	3.2 ± 0.2
	N 1s	triazine	0.8 ± 0.1	0.33 ± 0.05	3.1 ± 0.2	0.8 ± 0.2	0.32 ± 0.06	3.1 ± 0.2
	Br 2p	surface-bound	0.93 ± 0.03	0.93 ± 0.01	2.18 ± 0.03	0.93 ± 0.04	0.92 ± 0.02	2.18 ± 0.04
decoupled	C 1s	phenyl	0.29 ± 0.02	0.49 ± 0.02	5.85 ± 0.04	0.37 ± 0.03	0.51 ± 0.02	5.92 ± 0.04
		triazine	0.56 ± 0.09	0.51 ± 0.05	5.9 ± 0.2	0.7 ± 0.2	0.49 ± 0.07	5.9 ± 0.2
	N 1s	triazine	0.3 ± 0.2	0.44 ± 0.08	5.7 ± 0.2	0.5 ± 0.1	0.46 ± 0.06	5.8 ± 0.2
	Br 2p	surface-bound	0.90 ± 0.06	0.90 ± 0.03	2.12 ± 0.06	0.9 ± 0.2	0.90 ± 0.06	2.1 ± 0.2
	I 3d	surface-bound	0.97 ± 0.03	0.99 ± 0.01	2.32 ± 0.03	0.96 ± 0.03	0.99 ± 0.02	2.32 ± 0.03

5. Additional DFT results

5.1. Halogen adsorption heights

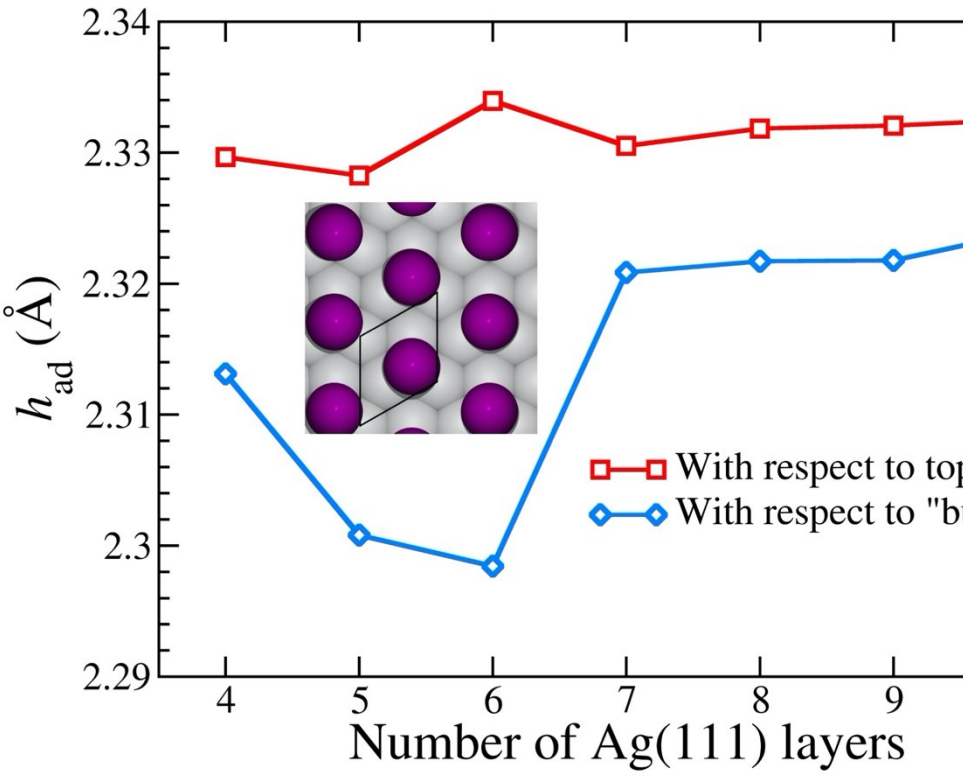

Fig. S8 Calculated iodine adsorption heights in a commensurate $\sqrt{3} \times \sqrt{3} \pm 30°$ monolayer on Ag(111) as a function of the number of layers in the slab. Iodine adsorbs in three-fold fcc hollow sites. Adsorption heights were calculated either with respect to the topmost Ag(111) layer (red data points and line) or with respect to the bulk (i.e. lowest Ag(111) layer, blue data points and line) according to Eq. (1). The monolayer structure is shown in the insert and the lines serve as guide to the eyes.

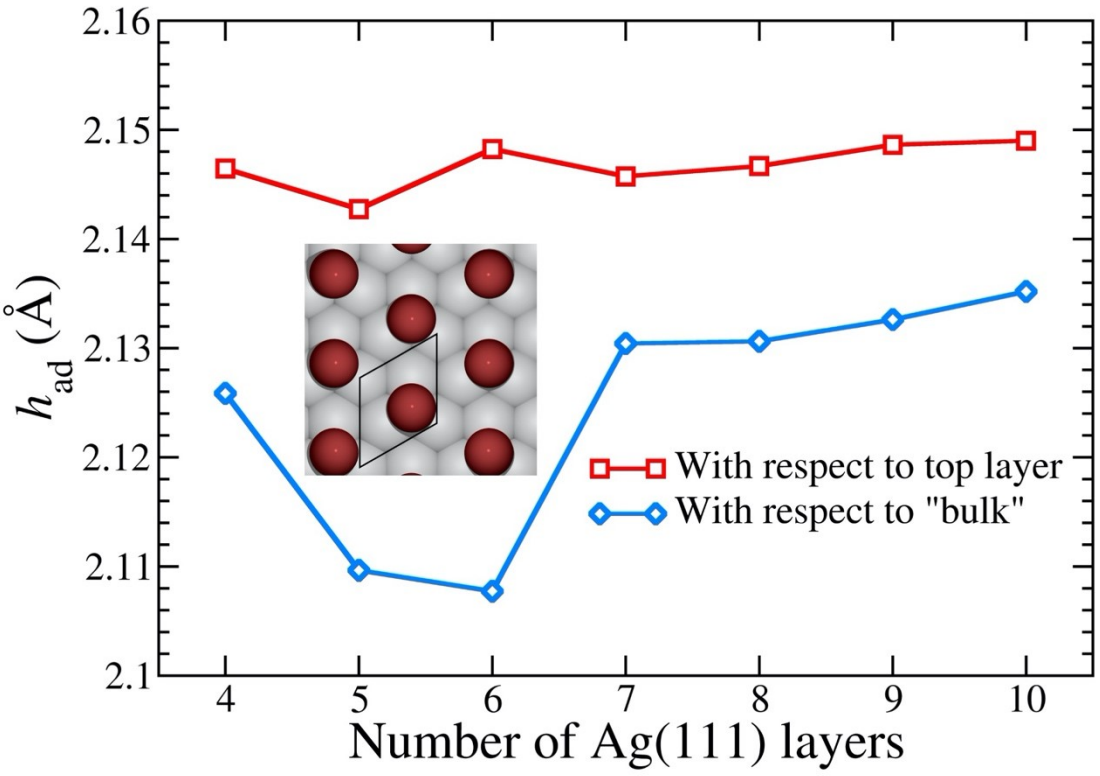

Fig. S9 Calculated bromine adsorption heights in a commensurate $\sqrt{3} \times \sqrt{3} \pm 30°$ monolayer on Ag(111) as a function of the number of layers in the slab. Iodine adsorbs in three-fold fcc hollow sites. Adsorption heights were calculated either with respect to the topmost Ag(111) layer (red data points and line) or with respect to the bulk (i.e. lowest Ag(111) layer, blue data points and line) according to Eq. (1). The monolayer structure is shown in the insert and the lines serve as guide to the eyes.

5.2. Free-standing covalent network

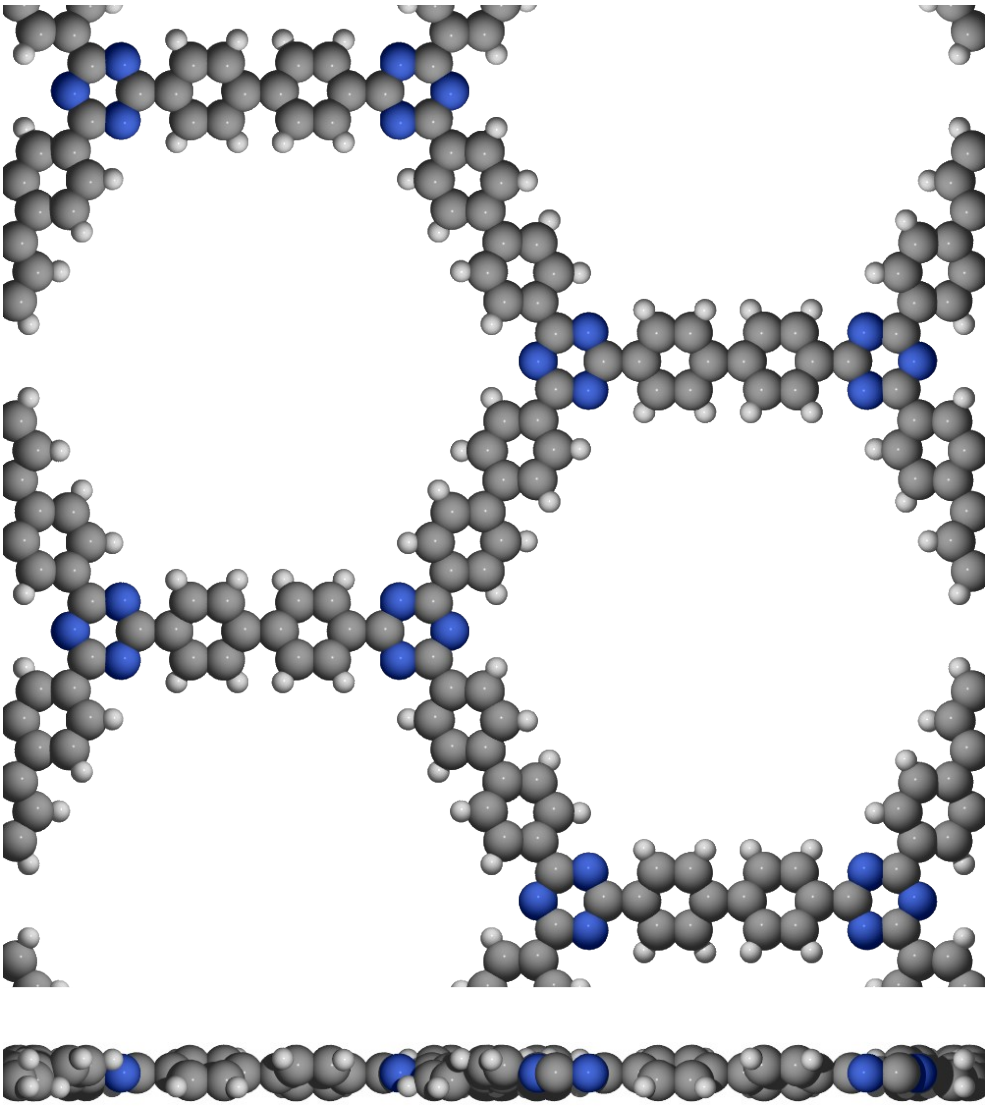

Fig. S10 DFT calculations of a free-standing covalent network. The upper part shows the top view, the lower part the side view. Optimization of the lattice parameter within a hexagonally constrained lattice results in a = b = 2.20 nm, which corresponds to a triazine-to-triazine distance of 1.27 nm. Steric hindrance between the *ortho*-hydrogen atoms results in phenyl tilt angles of 14.4° with respect to the network's plane. By contrast, calculations of a free-standing isostructural network that exclusively consists of phenyl rings yielded a larger phenyl tilt angle of 23°.[13] Accordingly, the mixed triazine-phenyl network is more planar owing to reduced steric hindrance at the triazine-phenyl linkages. The DFT calculated structure of the pure phenylene network is presented in the Supporting Information of ref. 13.

5.3. STM image simulations

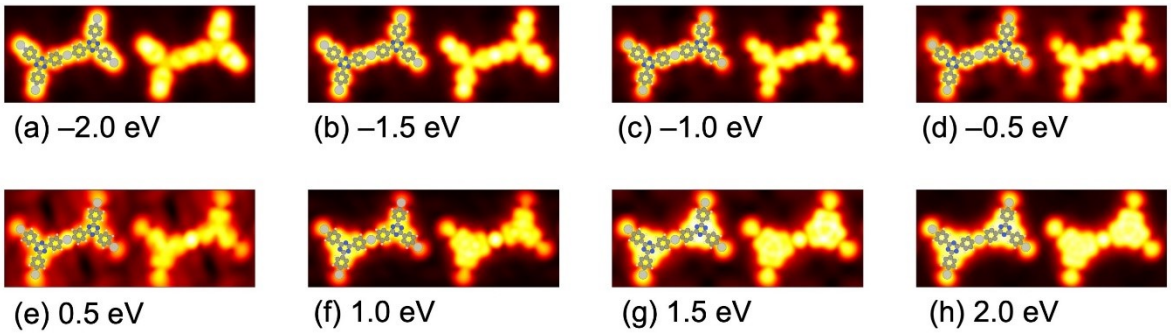

Fig. S11 STM image simulations for C-Ag-C bonded and Ag-terminated organometallic dimer on Ag(111) for a series of bias voltages. Therefore, electronic states were evaluated in the energy range between Fermi level and (a) -2.0 eV to (h) +2.0 eV as indicated. Structures were overlaid on the left-hand side. The Ag adatom in the C-Ag-C linkage appears bright, and depending on bias voltage, for instance for +1.0 eV, also brighter than the terminating Ag atoms at the periphery.

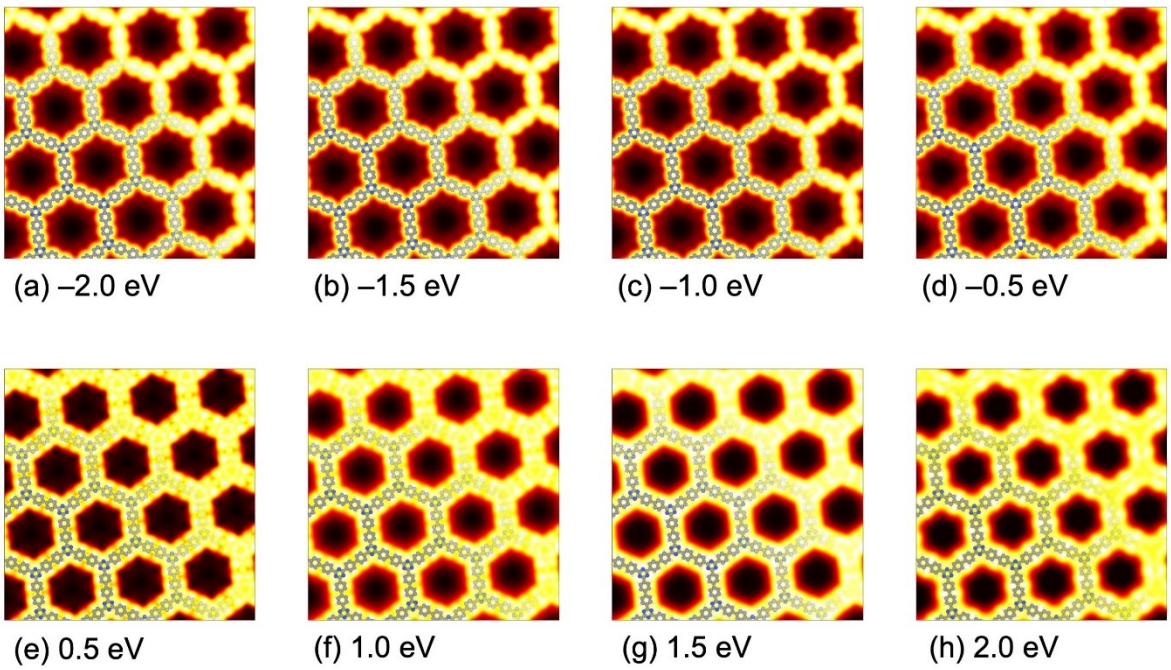

Fig. S12 STM image simulations of covalent networks directly on Ag(111) for a series of bias voltages. Therefore, electronic states were evaluated in the energy range between Fermi level and (a) -2.0 eV to (h) +2.0 eV as indicated. Structures of the covalent networks are overlaid at the lower left corner. Directly on Ag(111), the covalent networks do not show a pronounced internal STM contrast, only the central triazine rings appear slightly lower for certain bias voltages.

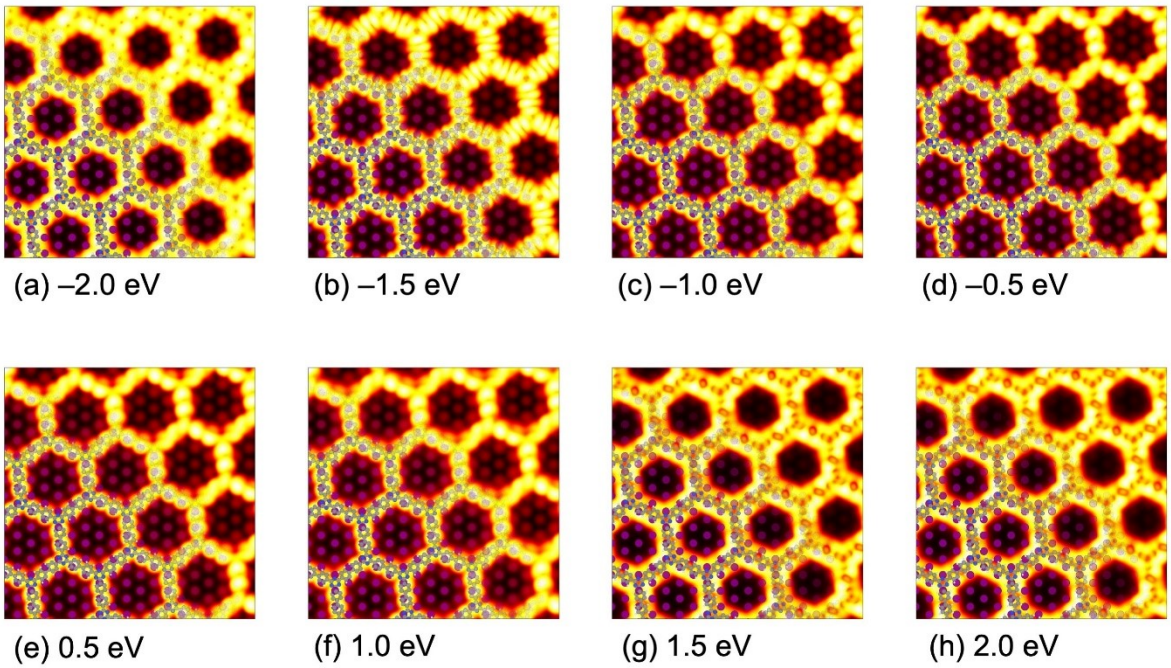

Fig. S13 STM image simulations of covalent networks on Ag(111) with an intercalated iodine monolayer for a series of bias voltages. Therefore, electronic states were evaluated in the energy range between Fermi level and (a) -2.0 eV to (h) +2.0 eV as indicated. Structures of both the covalent networks and the underlying iodine monolayers are overlaid at the lower left corner. After decoupling, the triazine rings appear as pronounced depressions and the connecting biphenyl spokes show internal structure. In agreement with the experiment, the close packed iodine monolayer can be recognized with the pores of the network.

6. Synthesis of TBPT

To a solution of trifluoromethanesulfonic acid (2.00 mL, 22.6 mmol) cooled to 0-10 °C, 4-bromo-benzonitrile (1.00 g, 5.49 mmol) was added in small portions. The reaction mixture was allowed to stir overnight at room temperature. The mixture was then transferred onto ice and neutralized with ammonium hydroxide. The solid was removed by filtration and washed with 100 mL of a 50/50 mixture of dichloromethane/acetone to remove unreacted nitrile, affording 980 mg of the product as colorless solid (1.79 mmol, 33% yield). MP > 300 °C (Lit. [14] 362-365 °C). IR (KBr): 3067, 1920, 1788, 1630, 1586, 1519, 1398, 1356, 1205, 1166, 1097, 1062, 1001, 838, 800, 552, 490 cm^{-1}. ^{1}H NMR (400 MHz, $CDCl_3$): δ 7.68 (d, ^{3}J = 8.4 Hz, 6H), 8.88 (d, ^{3}J = 8.4 Hz, 6H) ppm. Elemental analysis ($C_{21}H_{12}N_3Br_3$): Calcd. C, 46.19; H, 2.22; N, 7.70. Found C, 46.15; H, 2.11; N, 7.87.

7. References

1 Nečas, D. & Klapetek, P. Gwyddion: an open-source software for SPM data analysis. *Cent. Eur. J. Phys.* **10**, 181–188 (2012).

2 Lee, T. L. & Duncan, D. A. A Two-Color Beamline for Electron Spectroscopies at Diamond Light Source. *Synchrotron Radiat. News* **31**, 16-22 (2018).

3 Wojdyr, M. Fityk: a general-purpose peak fitting program. *J. Appl. Crystallogr.* **43**, 1126-1128 (2010).

4 Batterman, B. W. Effect of Dynamical Diffraction in X-Ray Fluorescence Scattering. *Phys. Rev.* **133**, A759-& (1964).

5 Woodruff, D. P. Surface structure determination using x-ray standing waves. *Rep. Prog. Phys.* **68**, 743-798 (2005).

6 Fisher, C. J. *et al.* Non-dipole photoemission effects in x-ray standing wavefield determination of surface structure. *J. Phys.-Condens. Mat.* **10**, L623-L629 (1998).

7 Kresse, G. & Furthmüller, J. Efficient iterative schemes for ab initio total-energy calculations using a plane-wave basis set. *Phys Rev B* **54**, 11169-11186 (1996).

8 Blöchl, P. E. Projector Augmented-Wave Method. *Phys Rev B* **50**, 17953-17979 (1994).

9 Dion, M., Rydberg, H., Schröder, E., Langreth, D. C. & Lundqvist, B. I. Van der Waals density functional for general geometries. *Phys. Rev. Lett.* **92** (2004).

10 Hamada, I. van der Waals density functional made accurate. *Phys Rev B* **89** (2014).

11 Tersoff, J. & Hamann, D. R. Theory and Application for the Scanning Tunneling Microscope. *Phys. Rev. Lett.* **50**, 1998-2001 (1983).

12 Lorente, N. & Persson, M. Theoretical aspects of tunneling-current-induced bond excitation and breaking at surfaces. *Faraday Discuss.* **117**, 277-290 (2000).

13 Rastgoo-Lahrood, A. *et al.* Post-Synthetic Decoupling of On-Surface-Synthesized Covalent Nanostructures from Ag(111). *Angew. Chem. Int. Ed.* **55**, 7650-7654 (2016).

14 Furukawa, H. *et al.* Isoreticular Expansion of Metal-Organic Frameworks with Triangular and Square Building Units and the Lowest Calculated Density for Porous Crystals. *Inorg Chem* **50**, 9147-9152 (2011).